Cell Biol Toxicol (2013) 29:39–58
DOI 10.1007/s10565-012-9236-8

ORIGINAL RESEARCH

Stress reaction of kidney epithelial cells to inorganic solid-core nanoparticles

Blanka Halamoda Kenzaoui · Catherine Chapuis Bernasconi · Lucienne Juillerat-Jeanneret

Received: 18 July 2012 / Accepted: 6 November 2012 / Published online: 19 November 2012

Abstract A route of accumulation and elimination of therapeutic engineered nanoparticles (NPs) may be the kidney. Therefore, the interactions of different solid-core inorganic NPs (titanium-, silica-, and iron oxide-based NPs) were studied in vitro with the MDCK and LLC-PK epithelial cells as representative cells of the renal epithelia. Following cell exposure to the NPs, observations include cytotoxicity for oleic acid-coated iron oxide NPs, the production of reactive oxygen species for titanium dioxide NPs, and cell depletion of thiols for uncoated iron oxide NPs, whereas for silica NPs an apparent rapid and short-lived increase of thiol levels in both cell lines was observed. Following cell exposure to metallic NPs, the expression of the tranferrin receptor/CD71 was decreased in both cells by iron oxide NPs, but only in MDCK cells by titanium dioxide NPs. The tight association, then subsequent release of NPs by MDCK and LLC-PK kidney epithelial cells, showed that following exposure to the NPs, only MDCK cells could release iron oxide NPs, whereas both cells released titanium dioxide NPs. No transfer of any solid-core NPs across the cell layers was observed.

Keywords Cytotoxicity · Epithelial kidney cells · Nanoparticles · Oxidative stress · Transepithelial transfer · Transferrin receptor/CD71

Abbreviations

Carboxy-H_2DCFDA	5/6-Carboxy-2,7-dichloro-dihydro-fluorescein
DAPI	4′,6′-Diamidino-2-phenylindole
DLS	Dynamic light scattering
HBSS	Hank's buffer solution
^{3}H-T	Tritiated thymidine
LY	Lucifer Yellow
MTT	3,4,5-Dimethylthiazol-yl-2, 5-diphenyl tetrazolium bromide
NEM	*N*-Ethyl-maleimide
NPs	Nanoparticles
ROS	Reactive oxygen species
TBHP	*tert*-Butyl hydroperoxide
TEER	Transepithelial electrical resistance
TEM	Transmission electron microscopy

Electronic supplementary material The online version of this article (doi:10.1007/s10565-012-9236-8) contains supplementary material, which is available to authorized users.

B. Halamoda Kenzaoui · C. Chapuis Bernasconi · L. Juillerat-Jeanneret (✉)
University Institute of Pathology,
Centre Hospitalier Universitaire Vaudois (CHUV),
rue du Bugnon 25,
CH1011 Lausanne, Switzerland
e-mail: lucienne.juillerat@chuv.ch

B. Halamoda Kenzaoui · C. Chapuis Bernasconi · L. Juillerat-Jeanneret
University of Lausanne (UNIL),
rue du Bugnon 25,
CH1011 Lausanne, Switzerland

USPIO	Ultrasmall superparamagnetic iron oxide

Introduction

Nanotechnology and the extended use of nanomaterials in nanomedicine is a rapidly developing field. Since the initial development of therapeutic nanoparticles (NPs), the field of nanotechnology has gained a lot of interest due to their huge potential for applications in industry and medicine. Nevertheless, a deep understanding of their interactions with living tissues and the knowledge of their possible effects in the human (and animal) body are necessary for the safe use of nanoparticulate formulations. Therefore, it is mandatory to ensure and control the biocompatibility of the components of therapeutic NPs to ensure that their intrinsic toxicity does not overtake their benefits. It is also necessary to understand their distribution in the human body, their biodegradation, and their excretion routes. However, the knowledge about possible interactions of engineered therapeutic NPs with living cells and tissues is presently not complete, and often the toxicological potential following exposure and the metabolic fate of NPs in living tissues and cells is not well defined (Caruthers et al. 2007; Heath and Davis 2008; Singh 2010).

Therapeutic NPs reach the systemic circulation after inhalation, ingestion, or intravenous injection. They may then disseminate to several organs, including the kidneys, which have been postulated as the probable final localizations and possible excretion route of NPs in living organisms (Longmire et al. 2008, 2011; Tang et al. 2009; Semete et al. 2010; Choi et al. 2011). The hypothesis of renal clearance of NPs originates from the known functions of the different tissue compartments of the kidney, and the renal processing of molecules, including macromolecules, involves the glomeruli acting as blood filters and the tubules which are able to transport solutes. While the glomerular filtration of NPs has been analyzed in some detail, knowledge on the interactions of NPs, in particular of metal-based solid-core NPs, with the kidney epithelia is currently limited. However, this knowledge is needed to gain information about the renal toxicity profile of NPs. Accumulation of silver or gold NPs in the glomeruli and in the basement membranes of renal tubules after inhalation or ingestion has been shown (Kim et al. 2009; Choi et al. 2011). Evaluation of the interaction of titanium dioxide, silica, and iron oxide NPs, as well as other NPs, with cells of the mesangium and proximal epithelium of the kidney has shown the potential harmful role of oxidative stress (L'Azou et al. 2008; Wang et al. 2009; Pujalté et al. 2011; Mahmoudi et al. 2011; Passagne et al. 2012). Thus, the evaluation of the effects of NP exposure on the functions of kidney cells of various subtypes, including of epithelial origin, needs further consideration.

As not only the size but also the chemical composition, surface chemistry and charge, and shape determine the behavior and clearance of NPs in a biological environment, different types of NPs must be compared to address these questions, in particular concerning NPs which have the potential to be used as therapeutic and diagnostic agents in nanomedicine. Ultrasmall super paramagnetic iron oxide (USPIO) NPs were developed for magnetic resonance imaging of the reticuloendothelial system, such as the liver, spleen, and lymph nodes, for perfusion imaging of the brain, myocardium, and kidney and for angiography and tumor vascular imaging and have been recently extended to new applications (Wang et al. 2001; Wu et al. 2004; Alexiou et al. 2006; Weinstein, et al. 2010). Fluorescent silica NPs have been widely applied in nanobiotechnology as new fluorescent nano-probes and biosensors, as drug delivery vehicles, and were also reported to be efficient tumor cell imaging agents (Wu et al. 2008; Lee et al. 2010; Liu et al. 2011). The use of titanium dioxide NPs in sunscreens and cosmetics has been extended to new applications in tissue engineering and biomaterials using their antibacterial properties for improving the properties of implant coatings (Yuan et al. 2010; Rupp et al. 2010).

In the present study, we used two widely studied epithelial kidney cell lines, the canine Madin Darby canine kidney (MDCK) cells, as a model for the renal distal tubular cells forming a very tight cellular barrier, and the porcine LLC-PK cells which are derived from the proximal tubule and form less tight epithelial cell layers. These cells present with cell–cell junctions and transport water, sodium, and calcium when seeded on semi-permeable supports and in confluent cell cultures form characteristic storage vesicles necessary for their water transport functions (Kuniaki et al. 2004). The interaction of selected inorganic solid-core (iron oxide-, silica-, and titanium dioxide-based) NPs was studied with these renal cells, determining their possible cytotoxicity, induction of an oxidative stress, and repression

of the expression of the transferrin receptor and questioning the subsequent release as well as the transfer across cell layers of the NPs by the kidney cells following exposure.

Methods

Nanoparticles

Uncoated ultrasmall superparamagnetic iron oxide nanoparticles (Fe_3O_4, uncoated USPIO NPs) were obtained from PlasmaChem (PlasmaChem GmbH Adlershof, Germany) as a ~3 % nanosuspension in water, average nanoparticle size 8±3 nm (as determined by dynamic light scattering (DLS)), zeta potential +15 mV in 10 mM NaCl, −23 mV in DMEM. The iron content was determined to be 18 mg iron/ml by quantitative Prussian Blue reaction according to a previously described protocol (Petri-Fink et al. 2005; Cengelli et al. 2010). Oleic acid-coated USPIO NPs (Fe_3O_4, 3 % oleic acid coating) were obtained from PlasmaChem as a ~7 % nanosuspension in water, average particle iron oxide core size 8±3 nm, hydrodynamic size 14–15 nm (determined by DLS), and zeta potential −30 mV at pH 7. The iron content was determined to be 206 mg iron/ml by quantitative Prussian Blue reaction. AminoPVA-coated USPIO NPs were prepared and characterized according to the protocol previously described (Petri-Fink et al. 2005). Briefly, ferrofluid was prepared by alkaline co-precipitation of ferric and ferrous chlorides, refluxed in nitric oxide–ferrous nitrate, and dialyzed, providing iron oxide nanoparticles (ferrofluid) of 9 nm. To obtain aminoPVA-coated USPIO NPs, the ferrofluid was mixed with poly (vinylalcohol, PVA), poly(vinylalcohol/vinylamine, aminoPVA) at a polymer-to-iron ratio of 10 and a PVA-to-aminoPVA copolymer ratio of 45 (mass ratios), resulting in aminoPVA-coated USPIO NPs of hydrodynamic diameter of 25 to 30 nm and a positive zeta potential of +25 mV. Titanium dioxide nanopowder (Aeroxide® TiO_2 P25) (TiO_2 NPs) was obtained from Evonik (Evonik Degussa GmbH, Hanau, Germany), average particle size 21 nm, large dispersion size, zeta potential −30 mV (Magdolenova et al. 2012). Fluorescent rhodamine-labeled silica nanospheres (25 nm fl-silica NPs and 50 nm fl-silica NPs) were obtained from Corpuscular as a 25-mg/ml suspension in water (Corpuscular, Inc, Cold Spring, USA) (17 and 12 mg/ml, respectively, as measured by thermogravimetric analysis by H Hofmann and P Bowen, LPT, EPFL), zeta potential −40 mV. The primary characteristics of the NPs have been previously published (Table 1 in Halamoda Kenzaoui et al. (2012b); Halamoda Kenzaoui et al. 2012a, 2012c; Magdolenova et al. 2012).

Cell lines and culture conditions

Canine MDCK epithelial cells and porcine kidney (LLC-PK) epithelial cells are available from the American Type Culture Collection (Manassas, VA, USA) and were grown in DMEM medium containing 4.5 g/l glucose, 10 % fetal calf serum, and penicillin/streptomycin antibiotics. All cell culture reagents were purchased from Gibco, Invitrogen, Basel, Switzerland. Cells were exposed to NPs in 250 μl of complete culture medium in 48-well plates (Costar, Corning, NY, USA) at decreasing concentrations, from 235 to 0.4 μg/ml NPs. Experiments were performed in triplicate wells at least twice in independent experiments. Means ± standard deviations (sd) were calculated. The interference of the NPs with the assays was evaluated and results were corrected when required.

Cell exposure to, association with, and release of USPIO NPs

Cells were grown in 48-well plates (Costar) until 75 % confluent and then exposed to USPIO NPs for the concentration and time indicated. The plates were washed three times with saline and analyzed for iron. Control cells without exposure to USPIO NPs were treated in the same conditions. To quantify cellular iron content, the cell layers were dissolved at room temperature for 1 h in 6 N HCl (125 μl/well of a 48-well plate); then, 125 μl of a 5 % solution of $K_4[Fe(CN)_6]\cdot 3H_2O$ (Merck, VWR international, Nyon, Switzerland) in H_2O was added for 10 min and the absorbance was measured at 690 nm in a multiwell plate reader (iEMS Labsystems, BioConcepts, Allschwil, Switzerland). A standard curve of $FeCl_3$ in 6 N HCl treated in the same conditions was used to quantify the amount of cell-bound iron. For release measurements following cell exposure to USPIO NPs, the cell layers were washed three times with PBS; complete DMEM medium without phenol red (Gibco) and without USPIO NPs was added to the cells for 24 h; then, 50 μl of culture medium was retrieved and iron content in the culture medium was analyzed. All experiments were

Table 1 Summary of results

Cell line	NPs[a]	Cytotoxicity[b] (MTT, DNA synthesis)	Oxidative stress[c]	Cell association/release[d]	Transfer across cell layers[d]
MDCK (canine distal tubule)	USPIO	Dose-dependent cytotoxicity of uncoated and OA-coated USPIO	No ROS production detected, uncoated USPIO: ↓ of thiol content in cells	Dose- and time-dependent cell association of uncoated and aminoPVA USPIO, followed by the release of uncoated USPIO	Transwell: no transfer of USPIO across cell layers, but internalization by the cells as observed by TEM
	TiO_2	↓ of mitochondrial metabolism after 48 and 72 h of exposure	↑ production of ROS	Measurement of cell association not possible, but the subsequent release detected by turbidimetry	Not measured
	Silica	Not cytotoxic, slight ↓ of DNA synthesis	No ROS production detected; ↑ of thiol content in cells after 4–24 h of exposure	Cell association at the highest applied concentration, no release	Transwell: no transfer detected, but presence of NPs in migrating cells as observed by TEM
LLC-PK (porcine proximal tubule)	USPIO	Uncoated USPIO: not cytotoxic, OA-coated USPIO: cytotoxicity at highest concentration	No ROS production detected, uncoated USPIO: ↓ of thiol content in cells	Dose- and time-dependent cell association of uncoated USPIO, no release, poor uptake of aminoPVA and OA-coated USPIO	Transwell: no transfer detected
	TiO_2	Not cytotoxic	↑ production of ROS	Measurement of cell association not possible, but the subsequent release detected by turbidimetry	Not measured
	Silica	Not cytotoxic, 25 nm: ↓ of DNA synthesis at max concentration	↑ of thiol content in cells after 4–24 h of exposure; ↓ of thiol content after 48 h of exposure	Cell association at the highest applied concentration, no release	Transwell: no transfer detected, but with presence of NPs in migrating cells as observed by TEM

[a] USPIO nanoparticles: uncoated, oleic acid-coated, and aminoPVA-coated; 25 and 50 nm silica fluorescent nanoparticles

[b] MTT assay; DNA synthesis measurement based on thymidine incorporation

[c] CarboxyH_2DCFDA assay for ROS production, Ddihydroethidium oxidation for superoxide anions detection, bromobimane assay for cellular thiol level evaluation

[d] Cell association, release, and transfer across cell layers quantified with the Prussian blue reaction (USPIO NPs) or with fluorescence measurement (silica NPs)

performed in triplicate wells and repeated at least twice. Means ± sd were calculated.

Histochemical determination of iron

After exposure to USPIO NPs, the cell layers were washed with saline and incubated for 20 min at room temperature with a 1:1 solution of 10 % HCl and 10 % $K_4[Fe(CN)_6]\cdot 3H_2O$ in H_2O, washed with distilled water, counterstained with Nuclear Fast Red (Merck, Darmstadt, Germany), dehydrated in graded ethanol to xylol, and mounted. Slides were photographed under a Nikon digital camera (DXM 1200, Nikon Corporation, Tokyo, Japan).

Cell exposure to and release of TiO_2 NPs

Cells were grown in 48-well plates (Costar) until 75 % confluent and then exposed to increasing concentrations of TiO_2 NPs for 24 h. The cell layers were washed three times with PBS; then, complete DMEM medium without phenol red (Gibco) and without NPs was added to the cells. After 72 h of washout, 200 μl of cell culture supernatant was retrieved and its absorbance at 540 nm was determined in a multiwell plate reader (iEMS Labsystems). All experiments were performed in triplicate wells and repeated at least twice. Means ± sd were calculated.

Cell exposure to, association with, and release of fluorescent silica NPs

Cells were grown in 48-well plates (Costar) until 75 % confluent and then exposed to silica NPs for the concentration and time indicated. Plates were washed twice with PBS and the fluorescence was measured in fresh PBS at $\lambda_{ex}/\lambda_{em}$=530/620 nm in a thermostated fluorescence plate reader (CytoFluor Series 4000, PerSeptive Biosystems, MA, USA). For release studies, the cells were incubated for another 24 h with fresh complete DMEM medium without NPs and without phenol red (Gibco); then, 200 μl of cell culture supernatants was transferred to another plate and the fluorescence was measured.

Fluorescence microscopy

Cells were grown for 24 h on glass slides (four-chamber Polystyrene Vessel Culture Slides, BD Falcon, Erembodegem, Belgium). Then, the medium was removed, and the silica NPs diluted in complete culture medium were added at the desired concentrations for a further 24 h. At the end of the exposure, the cell layers were washed in PBS, fixed in 4 % buffered paraformaldehyde for 20 min at 4 °C, washed in PBS, and incubated with 4′,6′-diamidino-2-phenylindole (DAPI) (Roche-Diagnostics, Rotkreuz, Switzerland, 1 μg/ml in PBS) for 30 min at 37 °C. The slides were washed with PBS and mounted in 20 % glycerol (Invitrogen) in PBS and then examined by fluorescence microscopy for DAPI labeling (Zeiss Axioplan 2, filters: $\lambda_{ex}/\lambda_{em}$=365/420 nm) and rhodamine-labeled silica NPs (Zeiss Axioplan 2, filters: $\lambda_{ex}/\lambda_{em}$=530/620 nm).

Evaluation of cell viability

Cells were grown in 48-well cell culture plates (Costar) until 75 % confluent and exposed to the NPs for the concentration and time indicated; then, the cell layers were washed in saline. Cell viability was evaluated using the 3,4,5-dimethylthiazol-yl-2,5-diphenyl tetrazolium bromide (MTT) assay (Sigma-Aldrich Buchs, Switzerland) added to the cells in fresh complete culture medium at 250 μg/ml final concentration for 2 h; then, the precipitated formazan was dissolved in 0.1 N HCl in 2-propanol and quantified at 540 nm in a multiwell plate reader (iEMS Labsystems). The interference of the NPs with the assay was controlled. All experiments were performed in triplicate wells and repeated at least twice. Means ± sd were calculated.

Evaluation of DNA synthesis

Following cell exposure to the NPs for 48 h, tritiated thymidine (^{3}H-T) (Amersham-Pharmacia, Glattbrugg, Switzerland, 400 nCi/mL final concentration) was added to the cells for 2–4 h. Then, the cell layers were precipitated with 10 % trichloroacetic acid and dissolved in 0.1 % sodium dodecyl sulfate (SDS) in 0.1 N NaOH, and scintillation cocktail (Optiphase HI-Safe, PerkinElmer, Beaconsfield, UK) was added. Radioactivity was counted with a β-counter (WinSpectra, Wallac, Germany). The radioactivity counts of treated cells were compared to the radioactivity counts of untreated cells. Experiments were conducted in triplicate wells and repeated twice. The interference of the NPs with the assay was controlled. Means ± sd were calculated.

Evaluation of ROS production

Free radical formation was determined with 5/6-carboxy-2,7-dichloro-dihydro-fluorescein (carboxy-H_2DCFDA). Cells were grown until confluent in 48 well-plates (Costar) and then preincubated for 40 min with carboxy-H_2DCFDA, (Molecular Probes, Invitrogen Basel, Switzerland; stock solution 25 mg/ml DMSO, final concentration 20 μM), washed, and incubated at 37 °C with the NPs diluted in enriched Hank's buffer solution containing 1.3 mM Ca^{2+}, 1.1 mMMg^{2+} and 5 mM glucose (HBSS; Gibco). *t*-Butyl hydroperoxide (TBHP; Sigma-Aldrich, 5 mM) was used as a positive control for free radical formation. The plate was immediately read at $\lambda_{ex}/\lambda_{em}$=485/530 nm in a thermostated fluorescence plate reader (CytoFluor) and then every hour for 4 h. All experiments were performed in triplicate wells and repeated at least twice. The interference of the NPs with the assay was controlled. Means ± sd were calculated.

Determination of cellular thiols

The monobromobimane assay was used to measure cellular thiol levels. Cells were grown until half-confluent in 48-well plates (Costar), exposed for 4, 24, or 48 h to the NPs, and washed with HBSS; then, 250 μl/well of 100 μM monobromobimane (Sigma-Aldrich) in HBSS was added at room temperature for 5 min in the dark. The cell layers were washed with HBSS and lyzed with 0.1 % Triton X-100 (Sigma-Aldrich) in HBBS. For a positive control for thiols consumption, the cells were exposed to 100 μM*N*-ethyl-maleimide (Sigma-Aldrich) for 1 min before the assay. The fluorescence was immediately read in a thermostated fluorescence plate reader (CytoFluor) at $\lambda_{ex}/\lambda_{em}$=485/580 nm. All experiments were performed in triplicate wells and repeated at least twice. The interference of the NPs with the assay was controlled. Means ± sd were calculated.

Transwell cultures

MDCK or LLC-PK cells (5×10^4 or 8×10^4 cells/cm^2, respectively) were seeded in 0.5 ml of complete medium in the apical upper compartment of Transwells® inserts (Costar, polyester membrane, pore diameter 3 μm, 12 inserts par plate); then, 1.5 ml of complete culture medium was added in the basal chamber. After 24, 48, 72, or 96 h of culture, the transepithelial electrical resistance (TEER) of the cell layers was measured at room temperature in complete culture medium with the Millicell-ERS voltohmmeter (according to the protocol of the provider, Millipore, MA, USA) in triplicates and the results were averaged; then, the transport of Lucifer Yellow (LY; see the following section) was performed at 37 °C to control for the increase in the cell layer tightness. Cells on the Transwells were examined using histological staining with methylene blue/azure and hematoxylin/eosin stains and immunocytochemical staining for occludin (see the following section). The evaluation of the transport of the NPs was performed after 72 h of culture when tightness was optimum.

Lucifer Yellow transfer

Both the apical and basal chambers of the Transwells were washed twice with HBSS containing 1.3 mM Ca^{2+} and 1.1 mMMg^{2+}, pH 7.4, preheated at 37 °C. LY (Sigma-Aldrich), final concentration 100 μM in HBSS, was added to the apical chamber and the devices were incubated at 37 °C. After 30, 60, 90, and 120 min, 200 μl of the solution from the basal chambers was removed and transferred into the wells of a 96-well plate for fluorescence reading and then replaced into the basal chamber. Fluorescence was determined in a thermostated fluorescence multiwell plate reader (CytoFluor) at $\lambda_{ex}/\lambda_{em}$=450/530 nm and compared with a standard curve of LY in HBSS at 37 °C.

Immunofluorescence

To examine for the presence of tight junctions in the cell layers, cells were grown for 72 h on Transwell membranes, fixed in 4 % buffered paraformaldehyde at 4 °C for 1 h, washed in PBS, permeabilized with cold methanol for 10 min at 4 °C, and incubated with 5 % bovine serum albumin (BSA; Sigma-Aldrich) in PBS for 1 h at room temperature. Antibody staining was performed with the monoclonal anti-occludin antibody conjugated to Alexa Fluor 488 (Molecular Probes, diluted 1:100 in 3 % BSA, 0.1 % Tween-20 in PBS) and incubated overnight at 4 °C. After washing in PBS, one drop of DAPI (Roche-Diagnostics, 1 μg/ml) was added; the slides were covered and sealed with nail polish and examined by fluorescence microscopy (Zeiss Axioplan 2, filters: $\lambda_{ex}/\lambda_{em}$=365/420 nm).

Transfer of NPs across renal cell layers

Both the apical chambers with kidney cells grown for 72 h and the basal chambers of the Transwells were washed twice with DMEM medium without phenol red (Gibco). Then, the apical chambers were filled with USPIO NPs (100 μg iron/ml) or fluorescent silica NPs (235 μg/ml) in DMEM without phenol red and the basal chambers with DMEM without phenol red. After 0, 2, 8, and 24 h of incubation, 50 μl of the medium from the basal chambers was removed and analyzed for iron oxide (Prussian Blue reaction) or rhodamine-silica (fluorescence) NPs content. The volume in the receiver chambers was maintained by adding 50 μl of fresh medium after each sampling. Parallel experiments were performed in the absence of cells (empty membranes). At the end of the experiment, the cells on the membrane inserts were washed three times with saline, detached with trypsin-EDTA (Gibco), centrifuged, and analyzed for iron content by the Prussian Blue reaction. All experiments were performed in triplicate wells and repeated at least twice, and means ± sd were calculated. The fluorescence of the silica NPs is not stable under the Transwell experimental conditions for more than 6 h; thus, the silica NP content of cells at the end of the experiments was not evaluated.

Transmission electron microscopy

MDCK and LLC-PK cells were grown on Transwell filters until confluent and then exposed to the NPs for the concentration and time indicated. At the end of the incubation, the cells were washed twice with PBS, fixed in 3 % glutaraldehyde in PBS (Sigma-Aldrich) for 24 h, and washed in cacodylate buffer. Samples were postfixed in 1.3 % osmium tetroxide in 0.2 M cacodylate buffer, pH 7.4, for 1 h and dehydrated in graded ethanol and then in propylene oxide and embedded in 50 % (*w*/*w*) epoxy embedding medium, 26 % (*w*/*w*) dodecenylsuccinic anhydride, 23 % (*w*/*w*) methyl nadic anhydride, 1 % (*w*/*w*) 2,4,6-tris(dimethylaminomethyl)phenol (DMP-30) (all from Fluka or Sigma-Aldrich). Blocks were cured for 48 h at 60 °C; thin sections (80–100 nm) were cut using an ultramicrotome (Ultracut E, Reichert-Jung Optische Werke AG, Wien, Austria) and mounted on 3-mm 200-mesh copper grids. Grids were stained for 75 min in saturated uranyl acetate solution (Fluka) and then for 100 s in lead citrate (Ultrostain 2, Laurylab, St Fons, France), examined, and photographed with a Philips CM10 transmission electron microscope combined with a MegaView III Soft Imaging system to document cell-associated USPIO NPs.

Western blot experiments

Cells were grown in 9-cm diameter Petri dishes (BD-Falcon) and exposed to the NPs (100 μg/ml, final concentration) for 24 h. Then, the cell layers were washed with cold PBS and lysed in 200 μL of lysis buffer (150 mM NaCl, 2 mM EDTA, 0.5 % Triton X-100, 50 mM Tris–HCl, 2 mM vanadate, 50 mM NaF, pH 7.2) and 10 μL of protease inhibitor cocktail (Sigma-Aldrich), scraped with a cell scrapper, extracted by three cycles of freeze/thawing and centrifuged at 10,000 rpm at 4 °C for 10 min. Supernatants were submitted to SDS-PAGE and transferred onto a nitrocellulose membrane (Whatman, Dassel, Germany). The membranes were blocked with 5 % fat-free milk in PBS, washed in 0.05 % Tween-20 (Sigma-Aldrich) in PBS, and incubated overnight at 4 °C with the goat polyclonal anti-transferrin receptor/CD71 antibody (Santa Cruz Biotechnology, CA, USA; diluted 1:5,000) and then exposed for 60 min to peroxidase-conjugated anti-goat antibody (Sigma-Aldrich, diluted 1:10,000) and visualized by chemiluminescence with the ECL detection kit (Amersham International PLC, Buckinghamshire, UK). To control for loading, the membranes were stripped by successive incubation in 0.1 M glycine, pH 2.3, 1 M NaCl in PBS, and 0.05 % Tween-20 in PBS, blocked for 1 h with 5 % fat-free milk in PBS, and exposed to the polyclonal anti-β-actin antibody (Sigma-Aldrich, diluted 1:5,000) for 1 h at room temperature followed by 1 h of incubation with peroxidase-conjugated anti-rabbit antibody (Promega, Wallisellen, Switzerland, diluted 1:20,000) and visualized by chemiluminescence (ECL, GE Healthcare, Amersham, UK).

Results

Cytotoxicity of the NPs for MDCK and LLC-PK cells

The MTT assay which measures the mitochondrial activity of viable cells was employed to evaluate the cytotoxicity of the NPs for the two kidney epithelial cell lines (Fig. 1). None of the tested NPs was highly cytotoxic. Only oleic acid-coated USPIO NPs, and to a

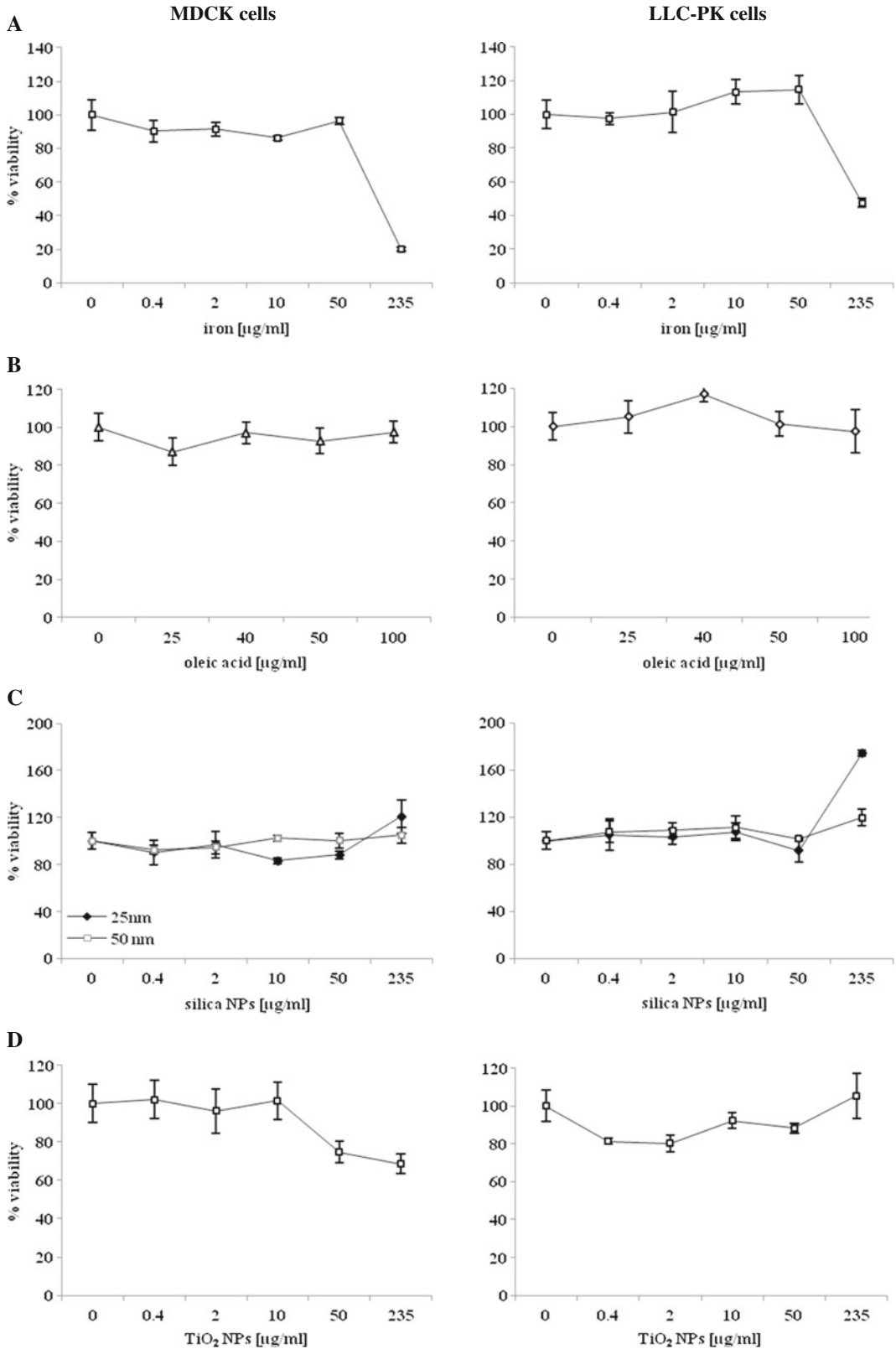
MDCK cells
LLC-PK cells
A
% viability
iron [µg/ml]
0 0.4 2 10 50 235
B
oleic acid [µg/ml]
0 25 40 50 100
C
25nm
50 nm
silica NPs [µg/ml]
D
TiO2 NPs [µg/ml]

◀ **Fig. 1** Cytotoxicity of NPs for MDCK and LLC-PK cells. Cytotoxicity for MDCK (*left*) and LLC-PK (*right*) cells of oleic acid-coated USPIO NPs (**a**), 25 and 50 nm (**c**), and TiO_2 NPs (**d**) NPs was assessed after 72 h of exposure using MTT assay. The cytotoxicity of free oleic acid at concentrations similar to its concentration in the oleic acid-coated USPIO NPs was also determined (**b**)

lesser extent TiO_2 NPs, were cytotoxic at the highest tested concentrations. Free oleic acid at concentrations corresponding to oleic acid concentrations of USPIO NPs was not cytotoxic for the cells (Fig. 1b).

The effect of cell exposure to the NPs on DNA synthesis was also determined using the thymidine incorporation assay (Fig. 2). Only oleic acid-coated USPIO and 25 nm fluorescent silica NPs decreased DNA synthesis in cells after 48 h of exposure. TiO_2 NPs did not induce any change in DNA synthesis. The LLC-PK cells were less sensitive than the MDCK cells to the NP effects.

Generation of an oxidative stress in MDCK and LLC-PK cells exposed to the NPs

The production of reactive oxygen species (ROS) in exposed cells was determined first using carboxy-dichloro-dihydro-fluorescein ester, which is internalized by the cells and oxidized to the fluorescent carboxy fluorescein by hydrogen peroxide and other ROS present in the cells. MDCK and LLC-PK cells produced only low amounts of ROS even when stimulated with TBHP as a positive control. Titanium dioxide NPs were the only NPs tested to induce the production of ROS in exposed MDCK and LLC-PK cells in amounts even higher than the levels resulting from treatment with TBHP (Fig. 3a).

After 24 or 48 h of exposure of the cells to the NPs, the cell content in cellular thiols, which are consumed during oxidative stress of cells, was also determined using the bromobimane assay. Uncoated USPIO NPs induced a significant decrease of cellular thiol content in MDCK cells and LLCPK cells after 24 and 48 h of exposure (Fig. 3b). Interestingly, both-sized fluorescent silica NPs induced an apparent rapid increase of thiol levels in both cell lines after 24 h of exposure and a decrease after 48 h of exposure, but only in LLC-PK cells (Fig. 3c; 25 nm fluorescent silica NPs, data for 50 nm fluorescent silica NPs not shown). Treatment of the cells with *N*-ethyl-maleimide was used as a positive control for thiol depletion in the cells.

Kidney cell association with and release of the NPs

First, the tight association of uncoated, oleic acid-coated, or aminoPVA-coated USPIO NPs with MDCK and LLC-PK cells was studied. Uncoated USPIO NPs agglomerated immediately in the cell culture medium, as previously reported (Halamoda Kenzaoui et al. 2012a, b, c), and the agglomerates precipitated on the bottom of the wells on the cell layers, enhancing direct contact between the cells and the NPs. Both aminoPVA-coated and oleic acid-coated USPIO NPs were stable in the cell culture medium and did not agglomerate during the experimental time frame exposure. The cell-associated iron content of USPIO NPs was determined using the histological Prussian Blue reaction (Fig. 4a). The cell-associated iron levels of the USPION NPs, as determined by quantitative Prussian Blue assay, increased time- and cell line-dependently and was proportional to the amount of NPs added (Fig. 4b). Oleic acid-coated USPIO NPs associated only poorly with MDCK and LLC-PK cells and the level of iron in the cell layers after 24 h of exposure was under the detection limit for quantitative measurement (data not shown). The tight association of aminoPVA-coated USPIO NPs was low after 4 h of exposure but increased significantly after 24 h of exposure to high concentrations (100 μg/ml and higher) of these NPs, particularly in MDCK cells (Fig. 4b).

Then, the release of iron following exposure to uncoated or aminoPVA-coated USPIO NPs by the kidney cells following cell exposure to the NPs was determined. In cells exposed to uncoated USPIO NPs, the release of iron by the cells was determined after a 24-h washout period following uptake (Fig. 5). A significant release of iron by MDCK cells but not by LLC-PK cells was observed (Fig. 5a, gray bars). The cell layers were also examined after the release experiment for the presence of iron and, whereas in the LLC-PK cell layers exposed to USPIO NPs iron was still present proportionally to the exposure NP concentrations, no detectable amounts of iron were found in the MDCK cell layers (Fig. 5a, black bars). The release of iron by MDCK and LLC-PK cells exposed to aminoPVA-coated USPIO NPs was not observed even with the highest concentrations of exposure (Fig. 5b).

The tight association of fluorescent 25 and 50 nm silica NPs with the cells was analyzed by fluorescence

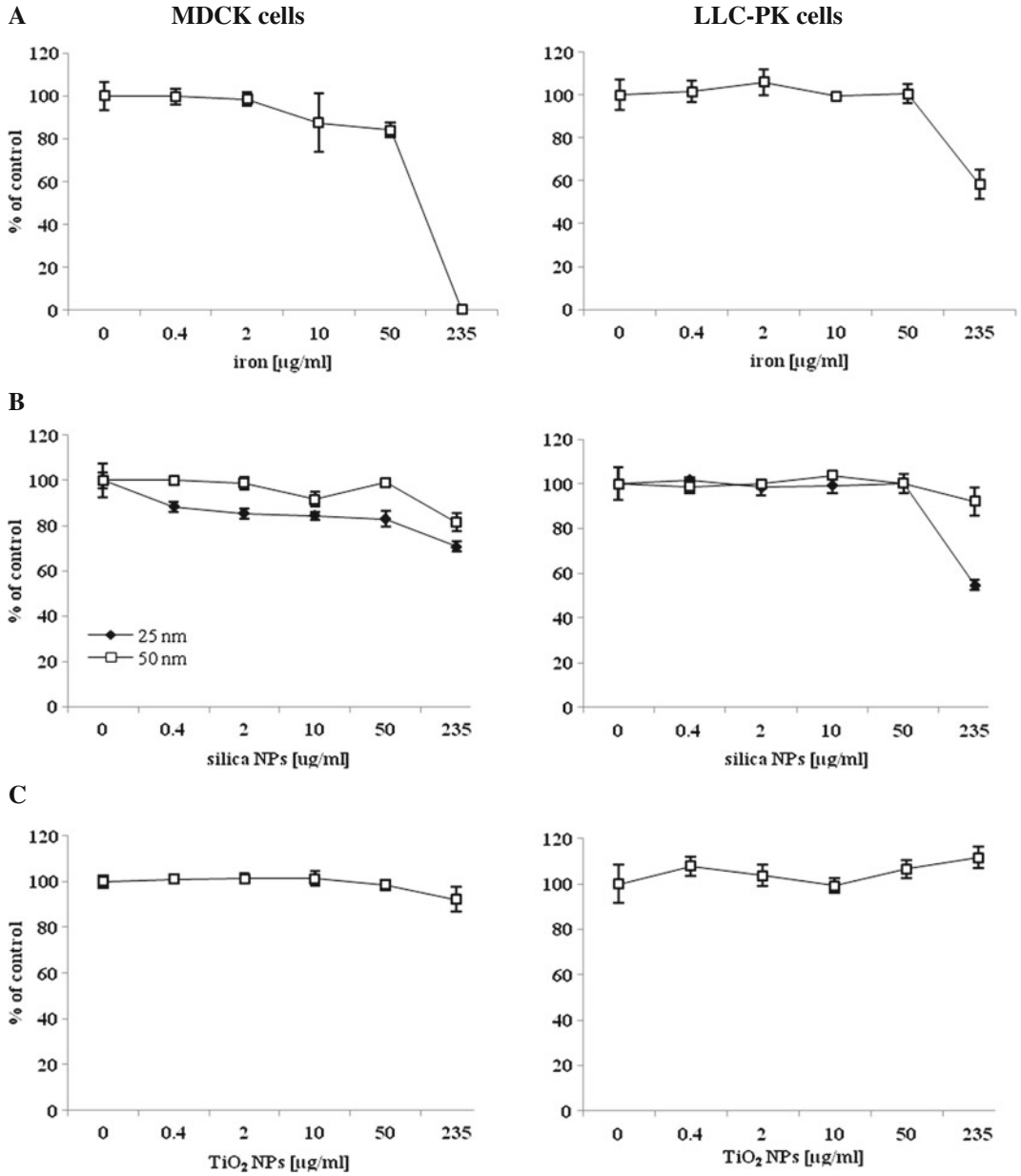

Fig. 2 Effect of NPs on DNA synthesis by MDCK and LLC-PK cells. DNA synthesis by MDCK (*left*) and LLC-PK (*right*) cells exposed either to oleic acid-coated USPIO NPs (**a**), 25 nm and 50 nm (**b**), or TiO_2 NPs (**c**) NPs was assessed after 48 h of exposure of the cells to the NPs

microscopy (Fig. 6a) and quantified as cell-associated fluorescence (Fig. 6b). With both techniques, the tight association of 25 nm silica NPs was detected only at the highest concentration tested (235 µg/ml), whereas for 50 nm silica NPs it was under the detection limits (data not shown). The release of 25 nm fluorescent silica NPs following exposure of MDCK or LLC-PK cells was not observed even at the highest exposure concentrations.

The quantification of tight association of TiO_2 NPs with the kidney cells was technically not possible. Following cell exposure to TiO_2 NPs, the release into the cell culture supernatants of light-absorbing particles was measured at 540 nm by turbidimetric

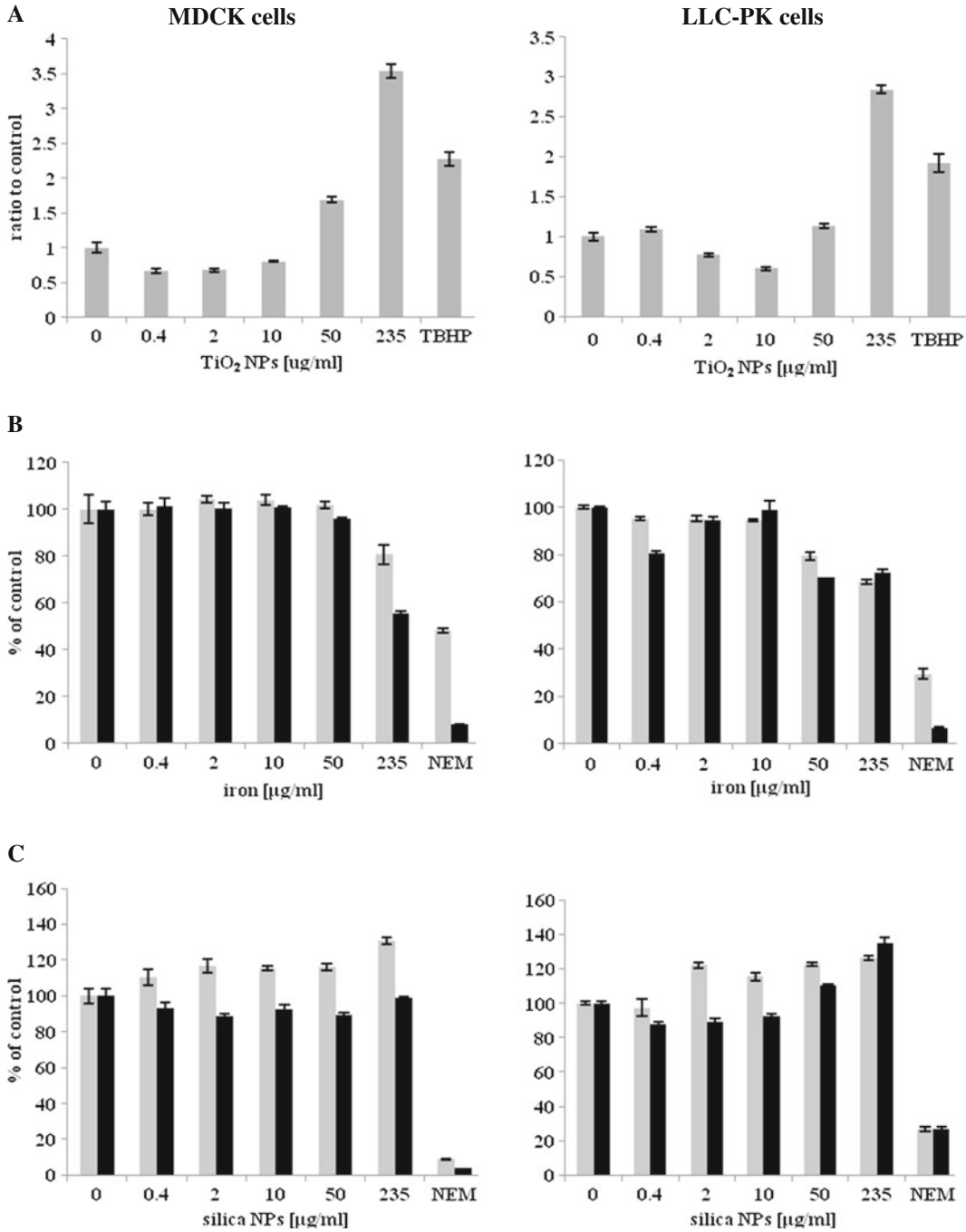

Fig. 3 Oxidative stress induced by the NPs in MDCK and LLC-PK cells. **a** The production of ROS in NP-exposed MDCK (*left*) and LLC-PK (*right*) cells was determined with the carboxyH_2DCFDA assay performed after 4 h of exposure of the cells to TiO_2 NPs. Treatment of cells with *tert*-butyl-hydroperoxide (*TBHP*) was used as a positive control. **b**, **c** Thiol levels were quantified using the bromobimane assay in MDCK cells (*left*) and LLC-PK cells (*right*) exposed to uncoated USPIO NPs (**b**) or to 25 nm silica NPs (**c**) for either 24 h (*gray bars*) or 48 h (*black bars*). Treatment of cells with *N*-ethyl-maleimide (*NEM*) was performed to deplete cells of thiols

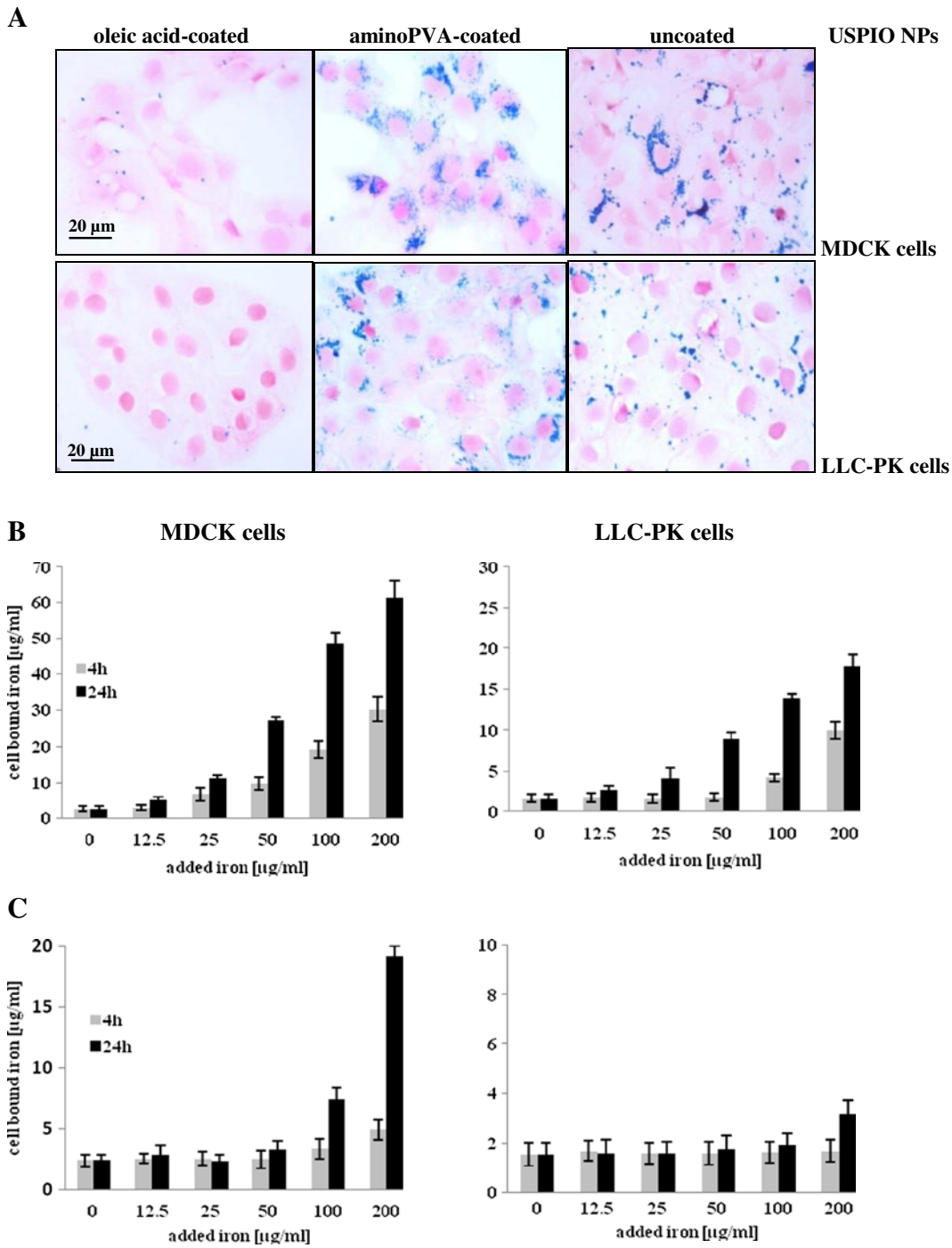

Fig. 4 Tight association of USPIO NPs with MDCK and LLC-PK cells. **a** The uptake of uncoated, oleic acid-coated, or aminoPVA-coated USPIO NPs (20 µg iron/ml) by MDCK (*left*) and LLC-PK (*right*) cells was visualized with the histological Prussian Blue and Nuclear Red staining (nuclei and cytoplasm: *pink*, iron: *blue*) after 24 h of exposure. **b**, **c** The uptake of uncoated USPIO NPs (**b**) and aminoPVA-coated USPIO NPs (**c**) by MDCK (*left*) and LLC-PK (*right*) cells was quantified with the Prussian Blue reaction after 4 and 24 h of exposure

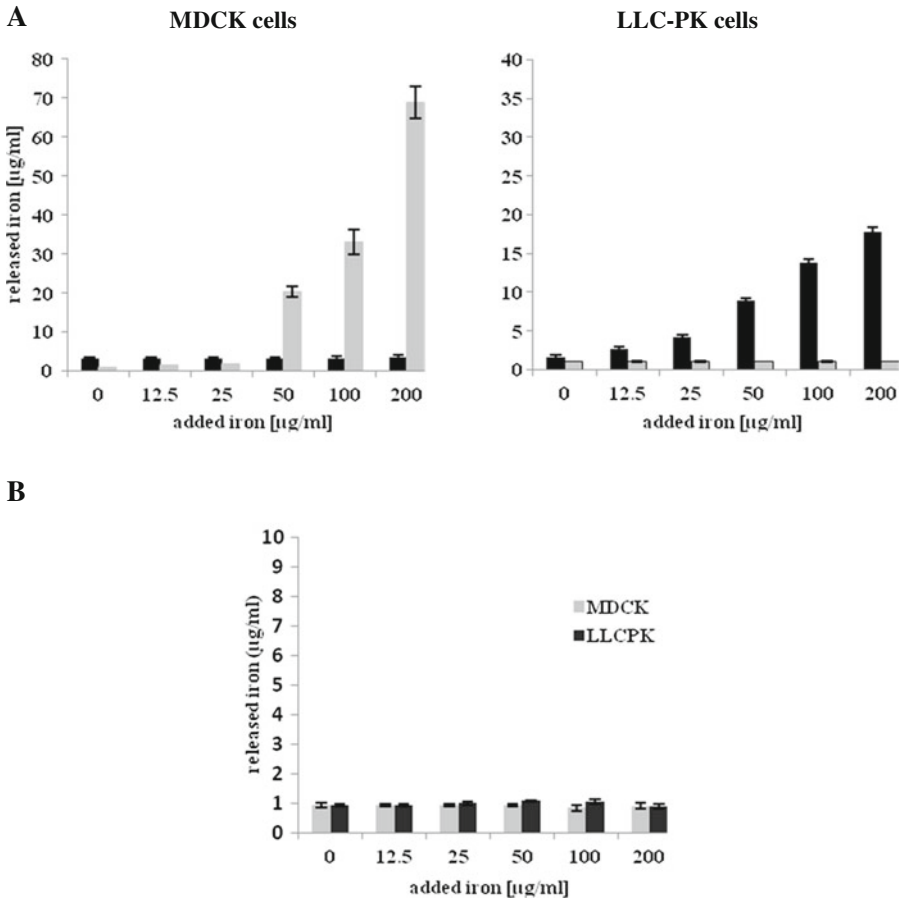

Fig. 5 Release of USPIO NPs by MDCK and LLCPK cells following exposure. **a** MDCK (*left*) and LLC-PK (*right*) cells were exposed to uncoated USPIO NPs for 24 h, washed with PBS, then incubated with fresh medium for another 24 h, and the iron concentration was quantified in the cell culture supernatants (*light gray bars*) and in the cell layer (*black bars*) with the Prussian Blue reaction. **b** MDCK (*light gray bars*) or LLC-PK (*dark bars*) cells were exposed to aminoPVA-coated USPIO NPs for 24 h, washed with PBS, then incubated with fresh medium for another 24 h, and the iron concentration was quantified in the cell culture supernatants with the Prussian Blue reaction

spectrophotometry. The cells did not release particles after 24 h of washout (results not shown); however, after 72 h, the release of particles by MDCK cells and LLC-PK cells was observed (Fig. 7).

Transfer of USPIO NPs across kidney cell layers

In order to evaluate if NPs can be transferred across monolayers of kidney cells, MDCK and LLC-PK cells were seeded on polyesther Transwell inserts; then, the confluence and permeability of the cell layers were examined after 24, 48, 72, and 96 h by hematoxylin/eosin histological staining of the cell layers on the membrane (Fig. S1a of the "Electronic supplementary material"). The permeability of the cell layers was examined by measuring the impairment of transfer of LY across the cell layers (Fig. S1b of the "Electronic supplementary material"), which was comparable in both cell lines, as well as the TEER (Fig. S1c of the "Electronic supplementary material"). TEER values for MDCK cell layers was ≥1,500 Ω cm^2 at 96 h post-seeding, as expected for the known properties of these cells to form very tight junctions and much higher than the electrical resistances of LLC-PK cells (~200 Ω cm^2). The presence of occludin, which is a protein participating in the formation of tight junctions, was observed in MDCK and LLC-PK cell layer at 72 h post-seeding (Fig. S1e of the "Electronic supplementary material"). As examined on transverse methylene blue/azure-stained histological slides of the cells on the Transwell membranes, MDCK cells formed a thick and tight cell layer, with several cells migrating across the pores toward the other side of the membrane, whereas the LLC-PK cell layer was thin, flat, less compact, and with only few cells migrating through the membrane (Fig. S1d of the "Electronic supplementary material"). The presence of junctions between the cells was demonstrated by transmission electron microscopy (TEM) at 72 h post-seeding (Fig. S2 of the "Electronic supplementary material"). MDCK cells formed tight junctions, visible especially at the top of the cell layer, whereas desmosomes were frequently present in both

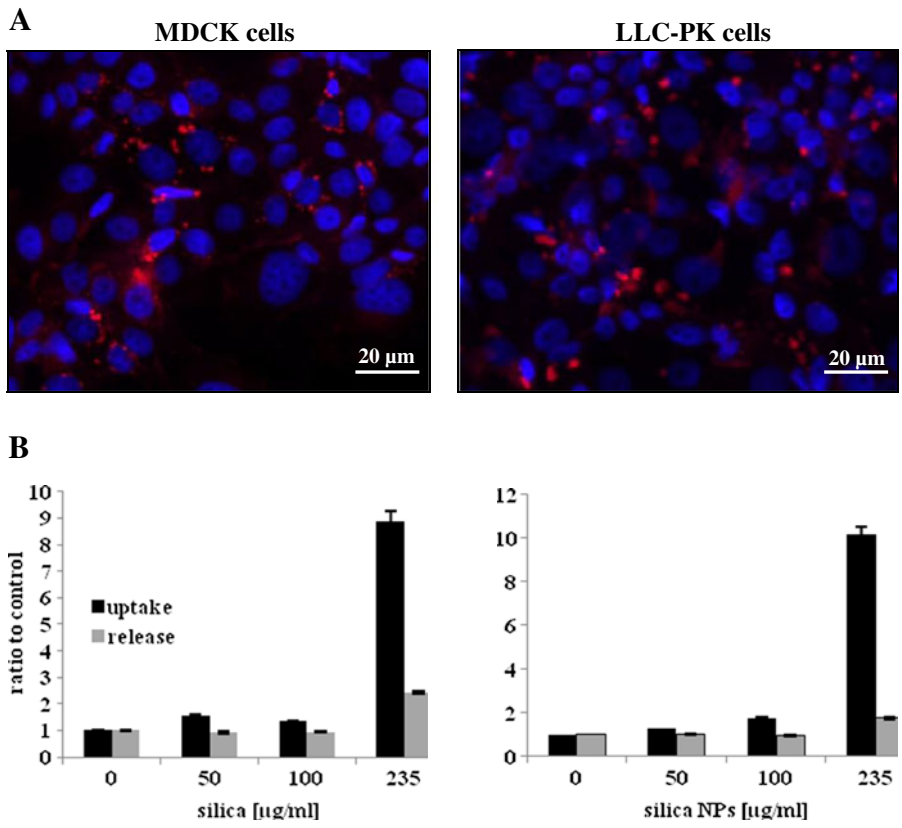

Fig. 6 Association and release of fluorescent silica NPs by MDCK and LLCPK cells. **a** Cellular uptake of 25 nm fluorescent silica NPs (200 µg/ml NPs) by MDCK (*left*) and LLC-PK (*right*) cells was determined after 24 h of exposure by fluorescence microscopy in cells stained with DAPI (nuclei fluoresce *blue*, rhodamine-labeled silica NPs fluoresce *red*). **b** Uptake by MDCK and LLC-PK cells of 25 nm silica NPs was quantified by cell-associated fluorescence (*black bars*) after 24 h of exposure. Then, the cells were incubated with fresh medium for another 24 h period and the fluorescence of NPs-associated rhodamine was quantified in the supernatant (*gray bars*)

cell lines. Thus, under our experimental conditions, these cells are representative of their expected epithelial functions in the kidney, and the interval between 72 and 96 h was chosen as optimal for performing the transfer experiments across confluent cell layers. The transfer of both oleic acid- and aminoPVA-coated USPIO NPs, which do not agglomerate under the experimental conditions, was studied during a 24-h time course (Fig. 8a). Neither oleic acid- nor aminoPVA-coated USPIO NPs were transferred across the renal cell layers, whereas both USPIO NPs were able to pass across the empty Transwell membranes. The iron content of the cell layers quantified at the end of the experiment (Fig. 8a, intracel) was low in MDCK cells exposed to oleic acid-coated USPIO NPs and higher in cells exposed to aminoPVA-coated USPIO NPs, whereas it was comparable in LLC-PK cells exposed to both USPIO NPs. TEM images of cells on the membranes after the transfer studies confirmed this information. MDCK cells demonstrated a tendency to migrate across the pores of the membrane; these migrating filipodia still loaded with NPs were visible in cell vacuoles of the migrating cells (Fig. 8b, right). The transfer by MDCK and LLC-PK cells of 25 and 50 nm fluorescent silica NPs was also investigated in two different media, DMEM or Ca/Mg-supplemented HBSS. We observed that under the Transwell experimental

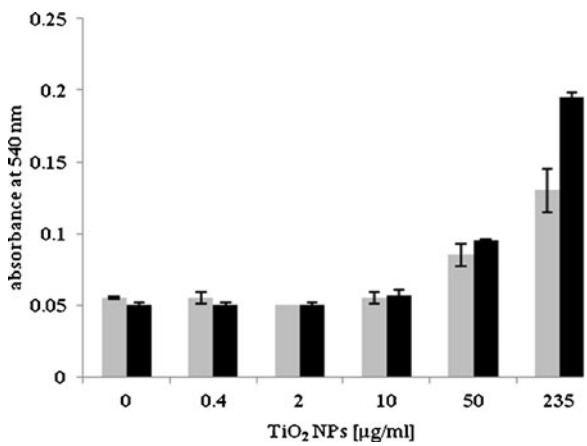

Fig. 7 Release of light-absorbing particles by MDCK and LLC-PK cells exposed to TiO_2 NPs. The release of particles by MDCK (*gray bars*) and LLC-PK (*black bars*) cells exposed to TiO_2 NPs for 24 h, then washed, and incubated with fresh medium for another 72 h was measured in the culture supernatants by turbidimetry

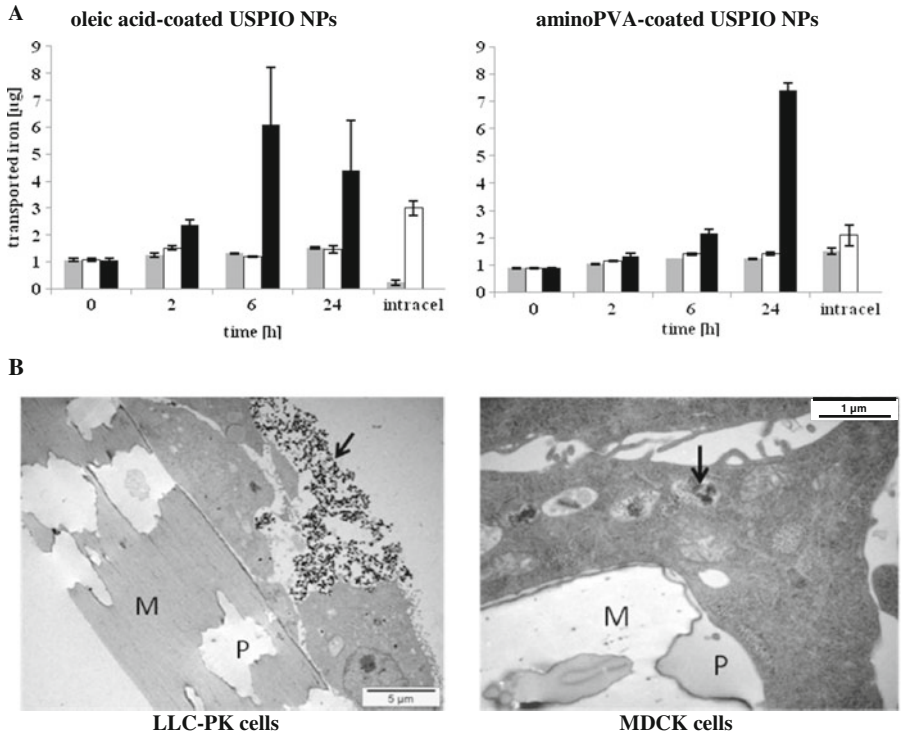

Fig. 8 Transfer of oleic acid-coated and aminoPVA-coated USPIO NPs across MDCK and LLC-PK cell layers. **a** Transfer of oleic acid-coated (*left*) and aminoPVA (*right*) USPIO NPs across confluent MDCK (*gray bars*) and LLCPK (*white bars*) cell layers and across the empty membranes (*black bars*). The iron content of the MDCK (*gray bars*, *intracel*) and LLC-PK (*white bars*, *intracel*) cell layers after the transfer study was also determined. The initial applied concentration of iron in the apical chamber was 100 µg/ml (50 µg of iron per Transwell), and the iron amount in the basal chamber was measured using the Prussian blue reaction. **b** TEM images of LLC-PK cells exposed to oleic acid-coated USPIO NPs (*left*) and MDCK cells exposed to aminoPVA USPIO NPs (*right*) for 24 h on the Transwell membrane. *M* membrane, *P* membrane pore, *black arrow* NPs

setting, but not under standard cell culture conditions, the fluorescent labeling of the NPs was not stable in both media and decreased rapidly after 6 h, limiting the time course of the transfer experiment to 6 h. Fluorescent 25 nm silica NPs crossed the empty Transwell membrane more efficiently than the 50 nm NPs; nevertheless, none of the silica NPs was transferred across confluent MDCK or LLC-PK cell layers for up to 6 h (Fig. 9a). The internalization of 25 nm fluorescent silica NPs by the cells on the Transwell membrane was confirmed by TEM (Fig. 9b).

Expression of the transferrin receptor by kidney cells exposed to iron oxide and titanium dioxide NPs

We have previously shown that the expression of the transferrin receptor/CD71, which contains an iron-responsive element in its promoter, is down-regulated when human cells are exposed to either aminoPVA-coated or uncoated USPIO NPs (Cengelli et al. 2010; Halamoda Kenzaoui et al. 2012b). Thus, we evaluated whether USPIO NPs as well as TiO_2 NPs, representing different solid-core metallic NPs compared to USPIO NPs, may have similar cellular consequences on this membrane iron transporter in kidney epithelial cells. The expression of the transferrin receptor/CD71 was determined by western blot in MDCK and LLC-PK cells exposed to either uncoated USPIO NPs or TiO_2 NPs (Fig. 10), two agglomerating NPs under the cell culture conditions. The results demonstrated that in MDCK cells the expression of the transferrin receptor/CD71 was down-regulated not only by the USPIO NPs but also by TiO_2 NPs, however at a lesser extent than iron oxide NPs. In LLC-PK cells, only USPIO NPs down-regulated the expression of the transferrin receptor/CD71. The results are summarized in Table 1.

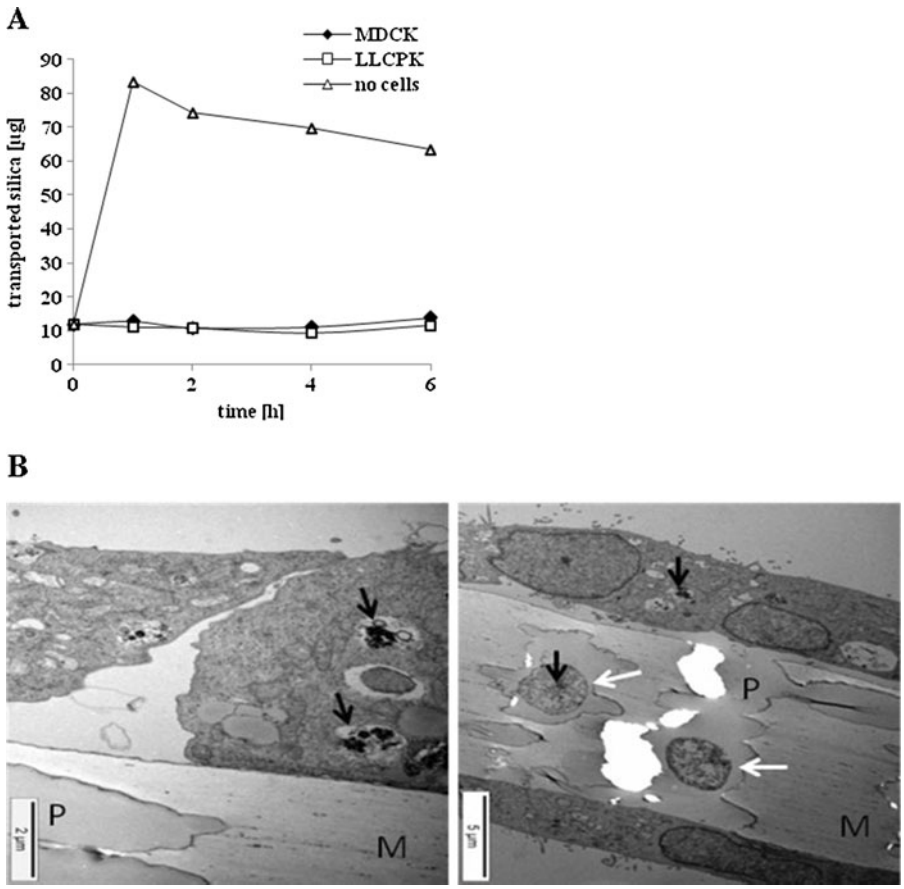

Fig. 9 Transfer of fluorescent silica NPs by MDCK and LLC-PK cells. **a** Transfer of fluorescent 25 nm silica NPs across MDCK (*black diamonds*) and LLC-PK (*open squares*) cell layers and in the absence of cells (*black triangles*). The initial concentration of silica NPs in the apical chamber was 235 μg/ml (117.5 μg NPs per Transwell), and the experiment was performed in HBSS buffer. **b** TEM images of LLC-PK cells exposed for 6 h to fluorescent 25 nm silica NPs on the Transwell membrane. *M* membrane, *P* membrane pore, *black arrow* silica NPs, *white arrow* cell fragments passing through the membrane pores

Discussion

The use of engineered nanoparticles in the industry and medicine has significantly increased, thus the potential for human exposure. This may pose a health concern since it has been shown in vitro and in vivo that NPs can induce adverse effects to cells and tissues (Wang et al. 2007; Napierska et al. 2009; Naqvi et al. 2010). It has to be emphasized that in vitro studies are necessary in the biological assessment of NPs so as to provide information concerning fundamental knowledge on biological targets and effects. However, the extrapolation of in vitro data for assessment of NPs needs to take into account the lack of knowledge on the uptake and distribution of NPs in organs in vivo. In vivo studies have shown that from the blood circulation, depending on their bio-physico-chemical properties, NPs can reach and accumulate in different organs such as the liver, spleen, kidneys, heart, or lungs (Jain et al. 2008; Tang et al. 2009; Semete et al. 2010). Kidney is particularly susceptible to xenobiotics, owing not only to its high blood supply but also to its ability to concentrate them for elimination. However, up to now, the impact of solid-core NPs for kidney epithelial cells has received little attention, and the

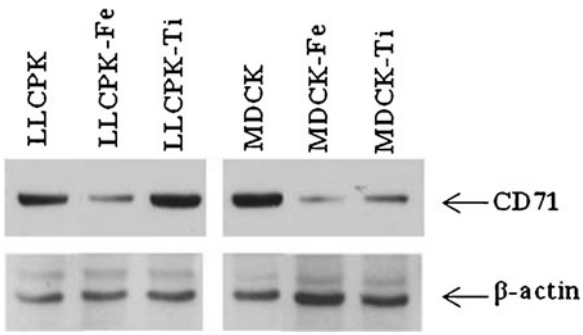

Fig. 10 Expression of the transferrin receptor/CD71 by MDCK and LLC-PK cells exposed to uncoated USPIO and TiO2 NPs. Cells were exposed to 100 μg/ml^2 NPs for 24 h; then, the expression of the transferrin receptor/CD71 and of β-actin as a loading control was determined by Western blotting in cell extracts

evaluation of NP effects on renal cells have only few reported precedents. Some in vivo experiments evidenced kidney damage, associated with morphological, pathological, and cellular changes leading to kidney dysfunction after exposure to NPs (Chen et al. 2006; Wang et al. 2007), while no pathological changes were found in rat kidneys after an intravenous administration of iron oxide magnetic NPs (Jain et al. 2008). The NP size-dependent cytotoxicity and oxidative stress generation induced by carbon nanotubes, titanium dioxide, and other metallic NPs in renal cells have also been assessed in vitro (L'Azou et al. 2008; Pujalté et al. 2011; Passagne et al. 2012). Increased levels of ROS production and some cytotoxicity were also observed in human embryonic kidney cells or proximal tubular cells exposed to silica NPs (Wang et al. 2009; Pujalté et al. 2011; Passagne et al. 2012), which might be inversely proportional to the size of silica NPs (Passagne et al. 2012). Cytoskeleton disruption and autophagy induction in LLC-PK renal cells by fullerenol NPs and quantum dots were reported (Stern et al. 2008; Johnson-Lyles et al. 2010).

To study the impact of engineered NPs in renal cells, we selected two epithelial kidney cell lines widely used for in vitro studies, originating either from the proximal (LLC-PK cells) or the distal (MDCK cells) tubules. We evaluated and compared their response to exposure to different types of inorganic solid-core NPs of interest for biomedical applications, titanium dioxide, two-sized silica NPs, and iron oxide (USPIO) NPs, either uncoated or coated with oleic acid or with aminoPVA. Except for uncoated USPIO NPs and TiO_2 NPs which agglomerated immediately and sedimented in the wells on the cell layers, the tested NPs were stable colloids in cell culture medium. The fluorescent 25 nm silica NPs associated with the cells at higher levels than the fluorescent 50 nm silica NPs, but none of these NPs was subsequently released by or transferred across the cells. Among the three USPIO NPs tested, the agglomerated uncoated USPIO NPs tightly associated with the cells more efficiently than the two coated USPIO NPs and, interestingly, they were subsequently released by MDCK cells, but not by LLC-PK cells. In these latter cells, the iron cores of the USPIO NPs were still cell-associated at 48 h post-exposure. On the contrary, both cells were able to release TiO_2 NPs following exposure. When seeded on semi-permeable membranes, MDCK cells formed a very tight and impermeable cell barrier, while the LLC-PK cell layer was less tight, these two cell lines together representing two different renal barrier models representative of their tissue of origin, the distal and the proximal tubules, respectively. However, whatever the model used, none of the NPs tested was able to cross these renal barrier models at a level sufficient to be detectable by the methods used. Nevertheless, the cells themselves were able to migrate across the pores of the membrane transporting the NPs with them.

We have previously shown, using human melanoma and brain endothelial cells (Cengelli et al. 2010; Halamoda Kenzaoui et al. 2012b), that USPIO NPs repress the expression of the transferrin receptor/CD71, a cell membrane protein involved in the import of iron into cells. The repression of the transferrin receptor/CD71 by uncoated USPIO NPs and TiO_2 NPs was observed only in MDCK cells, whereas in LLC-PK cells only uncoated USPIO NPs repressed this expression. Thus, not only the bio-physico-chemical properties of the NPs but also the characteristics of the epithelial cells are important for the cell responses to NP exposure. These results also suggest that repression of the transferrin receptor by metallic NPs is not restricted to iron-based NPs but may be possibly dependent on the cellular trafficking of the NPs. However, the repression of this transporter seems to be a general response to iron-based NPs in exposed cells, independent of the histological origin of the cells.

The cytotoxicity of the NPs was assessed with the MTT assay, reflecting the mitochondrial function in exposed cells, and DNA synthesis, reflecting the proliferative potential of the cells. Oleic acid-coated USPIO NPs, even if only poorly internalized by cells, were the most cytotoxic among the NPs tested, though not associated with the presence of free oleic acid potentially dissociating from the NPs. TiO_2 NPs also demonstrated some cytotoxicity in MDCK cells after long-term exposure. However, cytotoxicity for all NPs was observed only at the highest concentrations tested. The generation of ROS by NPs is generally considered to be a major contributor to NP cytotoxicity. ROS formation, when it exceeds the cellular antioxidant defensive capacity, represented mainly by cellular thiols such as glutathione, an essential antioxidant of cells (Gomes et al. 2005; Marquis et al. 2009), induces oxidative damage to biomolecules, including lipids, proteins, and DNA, ultimately leading to cell death. Oxidative stress can be monitored using dichlorofluorescein, detecting mostly hydrogen peroxide, and by monobromobimane, measuring the intracellular

level of thiols. In our study, only exposure to TiO_2 NPs induced elevated ROS production in both kidney cell lines without decreasing intracellular thiol levels, suggesting that the antioxidant adaptive cell response was not thiol-mediated. However, decreased cellular thiol levels were observed after exposure of the cells to uncoated USPIO NPs and 25 nm silica NPs, the NPs that were also able to decrease DNA synthesis in exposed cells, but which did not induce high oxidative stress. Thus, no direct relationship between oxidative stress response of the cells and cytotoxicity was observed. It has to be emphasized that MDCK cells were generally more sensitive to the effect of NPs than LLC-PK cells, providing a more sensitive model for evaluating the interactions of kidney epithelial cells with NPs. Using different kidney cells, from mesangial and proximal epithelial tubular origin, and titanium-, zinc-, or cadmium-based NPs, it was shown that aggregating ZnO and CdS NPs were cytotoxic and induced oxidative stress, resulting in GSH consumption, possibly mediated by NFκB nuclear translocation (Pujalté et al. 2011). Aggregating TiO_2 NPs were not cytotoxic, induced a low oxidative stress, and did not decrease GSH levels, confirming our results. As for our observations, the effects were cell dependent.

In conclusion, we have shown that inorganic solid-core NPs with a therapeutic interest (titanium dioxide NPs, silica NPs, iron oxide NPs) tightly associated with and were internalized by MDCK and LLC-PK kidney epithelial cells depending on the bio-physico-chemical characteristics of their coating and size, showing that (1) the size of NPs is important for interaction with the kidney epithelial cells, (2) the chemical composition of the solid core, metallic versus non-metallic, is also an important factor, (3) the potential for their dissolution in cells and modification of the oxidative state of the cells is a relevant issue, (4) the characteristics of the coating are also important, not only as ensuing stability versus agglomeration of the NPs but also most likely by modifying the corona of the NPs, and (5) the cell association/cell release of the NPs, very likely by regulating the amount of cell-associated components of the NPs, plays a fundamental role in the stress reaction of kidney epithelial cells to solid-core inorganic NPs. Following exposure, MDCK cells were able to release uncoated iron oxide and titanium dioxide NPs, but not aminoPVA-coated NPs or fluorescent silica NPs, two NPs tightly associated with the cells, whereas LLC-PK cells released exclusively titanium dioxide NPs following exposure. Even if some of the NPs were internalized by the cells, none of them was transferred as free NPs across either very tight (MDCK cells) or less tight (LLC-PK cells) kidney epithelial cellular barrier models. Nevertheless, we observed that both cells were able to migrate across semi-permeable membranes, transporting the NPs with them. The NPs were generally cytotoxic only at high concentrations, and only titanium dioxide NPs were able to generate oxidative stress, while iron oxide-based NPs depleted the cells of the antioxidative thiols, without measurable oxidative stress. The expression of the transferrin receptor/CD71, which contains an iron-responsive element in its promoter, is down-regulated when the iron content of cells increases. We had previously shown that the expression of the transferrin receptor/CD71 decreased, whereas lysosomal enzyme activation increased in cells exposed to USPIO NPs (Cengelli et al. 2010; Halamoda Kenzaoui et al. 2012c), suggesting that the iron oxide core of the USPIO NPs dissolved in the lysosomes of the cells and diffused out of these organelles to the nucleus. Similar results were observed in MDCK and LLC-PK cells with uncoated iron oxide NPs. In MDCK cells, but not in LLC-PK cells, however, titanium dioxide NPs also repressed the expression of the transferrin receptor/CD71, suggesting similar cell-specific repressive effects for these metallic NPs.

Acknowledgments The authors thank S. Güney-Ayra for excellent technical assistance and P. Bowen and H. Hofmann from EPFL, Lausanne, for providing the thermogravimetric analyses of the silica nanoparticles. This research was supported by a grant from the European Community 7th Framework Program (project no. 2007–201335 "NanoTEST").

Conflict of interest The authors have no relevant affiliation or financial involvement with any organization or entity with a financial interest or conflict concerning the information presented in this manuscript.

References

Alexiou C, Jurgons R, Seliger C, Iro H. Medical applications of magnetic nanoparticles. J Nanosci Nanotechnol. 2006;6:2762–8.

Caruthers SD, Wickline SA, Lanza GM. Nanotechnological applications in medicine. Curr Opin Biotechnol. 2007;18:26–30.

Cengelli F, Voinesco F, Juillerat-Jeanneret L. Interaction of cationic ultrasmall superparamagnetic iron oxide nanoparticles with human melanoma cells. Nanomedicine. 2010;5:1075–87.

Chen Z, Meng H, Xing G, Chen C, Zhao Y, Jia G, Wang T, Yuan H, Ye C, Zhao F, Chai Z, Zhu C, Fang X, Ma B, Wan L.

Acute toxicological effects of copper nanoparticles in vivo. Toxicol Lett. 2006;163:109–20.

Choi CH, Zuckerman JE, Webster P, Davis ME. Targeting kidney mesangium by nanoparticles of defined size. Proc Natl Acad Sci USA. 2011;108:6656–61.

Gomes A, Fernandes E, Lima JLFC. Fluorescence probes used for detection of reactive oxygen species. J Biochem Biophys Methods. 2005;65:45–80.

Halamoda Kenzaoui B, Vila MR, Miquel JM, Cengelli F, Juillerat-Jeanneret L. Evaluation of uptake and transport of cationic and anionic ultrasmall iron oxide nanoparticles by human colon cells. Int J Nanomedicine. 2012a;7:1275–86.

Halamoda Kenzaoui B, Chapuis Bernasconi C, Guney-Ayra S, Juillerat-Jeanneret L. Induction of oxidative stress, lysosome activation and autophagy by nanoparticles in human brain endothelial cells. Biochem J. 2012b;441:813–21.

Halamoda Kenzaoui B, Chapuis Bernasconi C, Hofmann H, Juillerat-Jeanneret L. Evaluation of uptake and transport of ultrasmall superparamagnetic iron oxide nanoparticles by human brain-derived endothelial cells. Nanomedicine. 2012c;7:39–53.

Heath JR, Davis ME. Nanotechnology and cancer. Annu Rev Med. 2008;59:251–65.

Jain TK, Reddy MK, Morales MA, Leslie-Pelecky DL, Labhasetwar V. Biodistribution, clearance, and biocompatibility of iron oxide magnetic nanoparticles in rats. Mol Pharm. 2008;5:316–27.

Johnson-Lyles DN, Peifley K, Lockett S, Neun BW, Hansen M, Clogston J, Stern ST, McNeil SE. Fullerenol cytotoxicity in kidney cells is associated with cytoskeleton disruption, autophagic vacuole accumulation, and mitochondrial dysfunction. Toxicol Appl Pharmacol. 2010;248:249–58.

Kim W, Kim J, Park JD, Ryu HY, Yu IJ. Histological study of gender differences in accumulation of silver nanoparticles in kidneys of Fischer 344 rats. J Toxicol Environ Health A. 2009;72:1279–84.

Kuniaki T, Yuk T, Toshiyuki M, Takeo A, Takeshi S, Ablimit A, Haruo H. Molecular mechanisms and drug development in aquaporin water channel diseases: water channel aquaporin-2 of kidney collecting duct cells. J Pharmacol Sci. 2004;96:255–9.

L'Azou B, Jorly J, On D, Sellier E, Moisan F, Fleury-Feith J, Cambar J, Brochard P, Ohayon-Courtès C. In vitro effects of nanoparticles on renal cells. Part Fibre Toxicol. 2008;5:22.

Lee KG, Wi R, Park TJ, Yoon SH, Lee J, Lee SJ, Kim Do H. Synthesis and characterization of gold-deposited red, green and blue fluorescent silica nanoparticles for biosensor application. Chem Commun. 2010;46:6374–6.

Liu Y, Lou C, Yang H, Shi M, Miyosh H. Silica nanoparticles as promising drug/gene delivery carriers and fluorescent nano-probes: recent advances. Curr Cancer Drug Targets. 2011;11:156–63.

Longmire M, Choyke PL, Kobayashi H. Clearance properties of nano-sized particles and molecules as imaging agents: consideration and caveats. Nanomedicine. 2008;3:703–17.

Longmire M, Ogawa M, Choyke PL, Kobayashi H. Biologically optimized nanosized molecules and particles: more than just size. Bioconjug Chem. 2011;22:993–1000.

Magdolenova Z, Bilanicova D, Pojana G, Fjellsbø LM, Hudecova A, Hasplova K, Marcomini A, Dusinska M. Impact of agglomeration and different dispersions of titanium dioxide nanoparticles on the human related in vitro cytotoxicity and genotoxicity. J Environ Monitor. 2012;14:455–64.

Mahmoudi M, Laurent S, Shokrgozar MA, Hosseinkhani M. Toxicity evaluation of superparamagnetic iron oxide nanoparticles: cell vision versus physicochemical properties of nanoparticles. ACS Nano. 2011;5:7263–76.

Marquis BJ, Love SA, Braun KL, Haynes CL. Analytical methods to assess nanoparticle toxicity. Analyst. 2009;134:425–39.

Napierska D, Thomassen LC, Rabolli V, Lison D, Gonzalez L, Kirsch-Volders M, Martens JA, Hoet PH. Size-dependent cytotoxicity of monodisperse silica nanoparticles in human endothelial cells. Small. 2009;5:846–53.

Naqvi S, Samim M, Abdin M, Ahmed FJ, Maitra A, Prashant C, Dinda AK. Concentration-dependent toxicity of iron oxide nanoparticles mediated by increased oxidative stress. Int J Nanomedicine. 2010;5:983–9.

Passagne I, Morille M, Rousset M, Pujalté I, L'Azou B. Implication of oxidative stress in size-dependent toxicity of silica nanoparticles. Toxicology. 2012;299:112–24.

Petri-Fink A, Chastellain M, Juillerat-Jeanneret L, Ferrari A, Hofmann H. Development of functionalized superparamagnetic iron oxide nanoparticles for interaction with human cancer cells. Biomaterials. 2005;26:639–46.

Pujalté I, Passagne I, Brouillaud B, Tréguer M, Durand E, Ohayon-Courtès C, L'Azou B. Cytotoxicity and oxidative stress induced by different metallic nanoparticles on human kidney cells. Part Fibre Toxicol. 2011;8:10.

Rupp F, Haup M, Klostermann H, Kim HS, Eichler M, Peetsch A, Scheideler L, Doering C, Oehr C, Wendel HP, Sinn S, Decker E, von Ohle C, Geis-Gerstorfer J. Multifunctional nature of UV-irradiated nanocrystalline anatase thin films for biomedical applications. Acta Biomater. 2010;6:4566–77.

Semete B, Booysen L, Lemmer Y, Kalombo L, Katata L, Verschoor J, Swai HS. In vivo evaluation of the biodistribution and safety of PLGA nanoparticles as drug delivery systems. Nanomedicine. 2010;6:662–71.

Singh S. Nanomedicine—nanoscale drugs and delivery systems. J Nanosci Nanotechnol. 2010;10:7906–18.

Stern S, Zolnik BS, McLeland CB, Clogston J, Zheng J, McNeil SE. Induction of autophagy in porcine kidney cells by quantum dots: a common cellular response to nanomaterials? Toxicol Sci. 2008;106:140–52.

Tang J, Xiong L, Wang S, Wang J, Liu L, Li J, Yuan F, Xi TJ. Distribution, translocation and accumulation of silver nanoparticles in rats. Nanosci Nanotechnol. 2009;9:4924–32.

Wang YXJ, Hussain SM, Krestin GP. Superparamagnetic iron oxide contrast agents: physicochemical characteristics and applications in MR imaging. Eur Radiol. 2001;11:2319–31.

Wang J, Zhou G, Chen C, Yu H, Wang T, Ma Y, Jia G, Gao Y, Li B, Sun J, Li Y, Jiao F, Zhao Y, Chai Z. Acute toxicity and biodistribution of different sized titanium dioxide particles in mice after oral administration. Toxicol Lett. 2007;168:176–85.

Wang F, Gao F, Lan M, Yuan H, Huang Y, Liu J. Oxidative stress contributes to silica nanoparticle-induced cytotoxicity

in human embryonic kidney cells. Toxicol In Vitro. 2009;23:808–15.

Weinstein JS, Varallyay CG, Dosa E, Gahramanov S, Hamilton B, Rooney WD, Muldoon LL, Neuwelt EA. Superparamagnetic iron oxide nanoparticles: diagnostic magnetic resonance imaging and potential therapeutic applications in neurooncology and central nervous system inflammatory pathologies, a review. J Cereb Blood Flow Metab. 2010;30:15–35.

Wu EX, Tang H, Jensen JH. Applications of ultrasmall superparamagnetic iron oxide contrast agents in the MR study of animal models. NMR Biomed. 2004;17:478–83.

Wu P, He X, Wang K, Tan W, Ma D, Yang W, He C. Imaging breast cancer cells and tissue using peptide-labeled fluorescent silica nanoparticles. J Nanosci Nanotechnol. 2008;8:2483–7.

Yuan Y, Ding J, Xu J, Deng J, Guo J. TiO_2 nanoparticles co-doped with silver and nitrogen for antibacterial application. J Nanosci Nanotechnol. 2010;10:4868–74.